frontiers in Materials

ORIGINAL RESEARCH
published: 28 September 2021
doi: 10.3389/fmats.2021.755332

Effects of Aromatic Thiol Capping Agents on the Structural and Electronic Properties of Cd_nTe_n (n = 6,8 and 9) Quantum Dots

Muhammad Imran[1], *Muhammad Jawwad Saif*[1]*, *Tahir Farooq*[1] *and Javed Iqbal*[2]

[1]Department of Applied Chemistry, Government College University Faisalabad, Faisalabad, Pakistan, [2]Department of Chemistry, University of Agriculture Faisalabad, Faisalabad, Pakistan

Thiols are efficient capping agents used for the synthesis of semiconductor and metal nanoparticles. Commonly, long-chain thiols are used as passivating agents to provide stabilization to nanoparticles. Theoretical methods rarely reported aromatic thiol ligands' effects on small-sized CdTe quantum dots' structural and electronic properties. We have studied and compared the structural and electronic properties of (i) bare and (ii) aromatic thiols (thiophenol, 4-methoxybenzenethiol, 4-mercaptobenzonitrile, and 4-mercaptobenzoic acid) capped Cd_nTe_n quantum dots (QDs). Aromatic thiols are used as thiol-radical because of the higher tendency of thiol-radicals to bind with Cd atoms. This work provides an understanding of how the capping agents affect specific properties. The results show that all aromatic thiol-radical ligands caused significant structural distortion in the geometries. The aromatic thiol-radical ligands stabilize LUMOs, stabilize or destabilize HOMOs, and decrease HOMO-LUMO gaps for all the capped QDs. The stabilization of LUMOs is more pronounced than the destabilization of HOMOs. We also studied the effect of solvent on structural and electronic properties. TD-DFT calculations were performed to calculate the absorption spectra of bare and capped QDs, and all the capping ligands resulted in the redshift of absorption spectra.

Keywords: CdTe, DFT-density functional theory, capping agent effect, electronic properties, thiols

OPEN ACCESS

Edited by:
Ke-Qiu Chen,
Hunan University, China

Reviewed by:
Jianguang Feng,
Qingdao University of Science and Technology, China
Mustafa Kurban,
Ahi Evran University, Turkey

***Correspondence:**
Muhammad Jawwad Saif
jawwadsaif@gmail.com

Specialty section:
This article was submitted to Quantum Materials, a section of the journal Frontiers in Materials

Received: *08 August 2021*
Accepted: *13 September 2021*
Published: *28 September 2021*

Citation:
Imran M, Saif MJ, Farooq T and Iqbal J (2021) Effects of Aromatic Thiol Capping Agents on the Structural and Electronic Properties of Cd_nTe_n (n = 6,8 and 9) Quantum Dots. Front. Mater. 8:755332. doi: 10.3389/fmats.2021.755332

INTRODUCTION

Semiconductor quantum dots (QDs), or "nanoclusters," or "nanoparticles" of CdTe and CdSe, are gaining significant attention due to their potential applications in various fields. Optoelectronic devices (Talapin et al., 2010; Kumar and Rao, 2014; Kershaw et al., 2017) (e.g., LEDs (Anikeena et al., 2009; Zou et al., 2017), sensors (Liang et al., 2014; Kanagasubbulakshmi et al., 2018), solar cells (Yaacobi-Gross et al., 2012; Huang et al., 2014; Carey et al., 2015; Bosio et al., 2017; Xiao et al., 2018), photodetectors (Barkhouse et al., 2008; Tu and Lin, 2008; Amelia et al., 2012)) and biomedical devices (Zheng et al., 2007; Yaghini et al., 2009; He and Ma, 2014) use QDs owing to their unique properties: size tunability, changeable surface chemistry (through capping with variety of ligands) (Hines and Kamat, 2013; Hines and Kamat, 2014), photoluminescence and absorption profile (Wuister et al., 2003; Wuister et al., 2004; Weng et al., 2006; Duan et al., 2009). The surface chemistry of semiconductor QDs is important in determining the electronic and structural properties because of their large surface-to-volume ratio.

The synthesis of semiconductor QDs is carried out in various ways, among which aqueous synthesis has considerable advantages in terms of high yield, reproducibility, and selectivity. During the synthesis of QDs, capping ligands tend to cover the surface of newly synthesized QDs and alter the structural and electronic properties of QDs. Ligands-capped CdTe QDs exhibit unique tunable structural, emission, and electronic properties (Akamatsu et al., 2005; Guo et al., 2005; Yaacobi-Gross et al., 2012; Deng et al., 2013; Lin et al., 2014; Amin et al., 2015; Liu et al., 2015; Schnitzenbaumer and Dukovic, 2018).

The presence of ligands on the surface affects the nucleation and growth of QDs considerably. Knowing the ligand effect helps develop a strategy for the synthesis and manipulating the size and properties of the QDs. Experimental characterization of structures and properties during the synthesis process remains challenging due to the minimal size and short lifetime of newly formed particles of QDs. On the other hand, first-principles computational techniques have been a good instrument for investigating the structures and properties of QDs. The cluster models have been used in several theoretical studies to investigate the structural and electronic properties of bare and ligated CdSe/CdTe QDs (Bhattacharya and Kshirsagar, 2007; Bhattacharya and Kshirsagar, 2008; Wang et al., 2009; Xu et al., 2010a; Seal et al., 2010; Haram et al., 2011; Kuznetsov et al., 2012; Lim et al., 2012; Ma et al., 2012; Leubner et al., 2013; Lin et al., 2013; Sriram and Chandiramouli, 2013; Wu et al., 2013; Alnemrat et al., 2014; Kuznetsov and Beratan, 2014; Rajbanshi et al., 2014; Sarkar et al., 2014; Shah and Roy, 2014; Aruda et al., 2016; Kilina et al., 2016; Swenson et al., 2016; Cao et al., 2018). Mainly, these studies were limited to exploring the capping effects of aliphatic ligands on the structural, electronic, and optical properties of CdTe QDs. Most of these computational studies have been conducted on small-sized QDs because of significant challenges associated with the atomistic simulation of large-sized QDs (Bhattacharya and Kshirsagar, 2007; Wang et al., 2009; Seal et al., 2010; Ma et al., 2012). These studies determined the possible lowest energy structures and optical properties of Cd_nTe_n (n = 1–16, 19, 20, 24, 28) nanoclusters employing the first-principles calculations.

Recent computational and experimental studies have confirmed the utilization of aromatic capping ligands in synthesis and the capping exchange process of CdSe/CdTe QDs (Bloom et al., 2013; Lin et al., 2013; Kumar et al., 2015; Aruda et al., 2016; Swenson et al., 2016). However, significant and systematic studies that would have investigated the effect of aromatic ligands on the structural, electronic, and optical properties of CdTe QDs are rare. Hence, the present study aims to fill that knowledge gap and provide a systematic computational analysis of the structural, electronic, and optical properties of aromatic thiol capped CdTe QDs.

In one of our previous studies, we had performed an extensive search for the lowest energy geometries of Cd_nTe_n QDs (n = 1–17) using particle swarm optimization (PSO) algorithms and density functional theory (DFT) approaches and explored structural and electronic properties (Imran et al., 2019). The present study presents structural and electronic properties of bare and capped small-sized Cd_nTe_n (n = 6,8 and 9) QDs. We have used four aromatic thiol ligands for capping: thiophenol (TP), 4-methoxybenzene-thiol (MBT), 4-mercaptobenzonitrile (MBN), and 4-mercaptobenzoic acid (MBA) (see **Figure 1**).

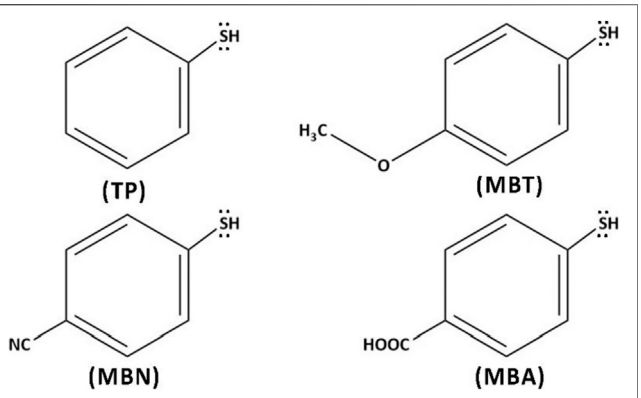

FIGURE 1 | Structures of the capping ligands: thiophenol (TP), 4-methoxybenzenethiol (MBT), 4-mercaptobenzonitrile (MBN), and 4-mercaptobenzoic acid (MBA).

Computational Methods

All the calculations described here were performed using the Gaussian 09W package (Frisch et al., 2013). Recent studies have used the simulated annealing technique to find CdTe clusters' lowest energy structures (Wang et al., 2009; Ma et al., 2012). Our previous study performed an extensive structural search for CdTe clusters using PSO algorithms as implemented in CALYPSO, evaluated the candidate clusters by DFT and MP2 theory levels. We re-used the lowest energy CdTe structures from our previous work for the sake of the present work (Imran et al., 2019). All the

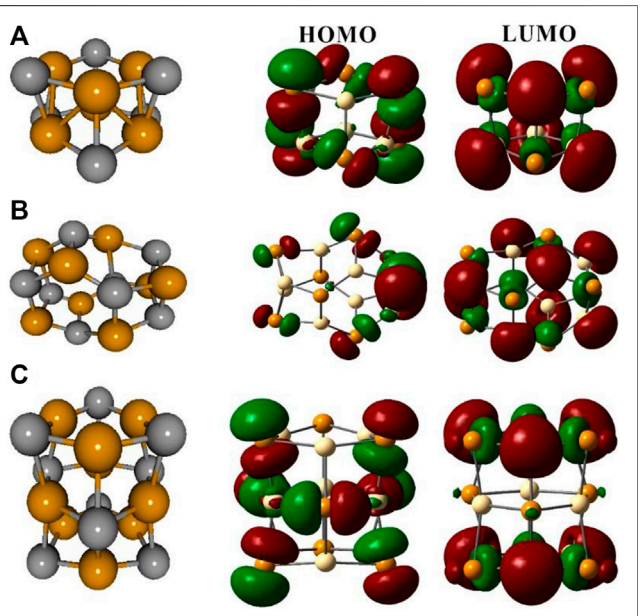

FIGURE 2 | Optimized gas-phase structures and Frontier orbitals of bare Cd_6Te_6 **(A)**, Cd_8Te_8 **(B)** and Cd_9Te_9 **(C)** QDs. Dark yellow spheres represent Cd, and gray spheres represent Te.

TABLE 1 | Calculated E_{HOMO} and E_{LUMO} energies (eV), HOMO-LUMO gaps (eV) of bare Cd_nTe_n (n = 6, 8, and 9) QDs in the gas phase, and toluene with B3LYP/Lanl2dz approach.

Species (symmetry, spin state)	E_{HOMO}, eV (gas phase; toluene)	E_{LUMO}, eV (gas phase; toluene)	Gap, (eV)
Cd_6Te_6 (C_{3v} ^1A)	–6.150	–3.10	3.05
	–5.96	–2.86	3.10
Cd_8Te_8 (S_4 ^1A)	–6.19	–3.10	3.09
	–6.01	–2.89	3.12
Cd_9Te_9 (D_{3h} ^1A)	–5.93	–3.17	2.76
	–5.74	–2.86	2.88

TABLE 2 | Calculated E_{HOMO} energy (eV), E_{LUMO} energy (eV), HOMO-LUMO gaps (eV), excitation energies (E_{max}) (eV), and maximum absorption wavelengths (λ_{max}) (nm), of the excited states with maximum oscillator strength of bare Cd_nTe_n (n = 6, 8, and 9) QDs in the gas phase and toluene with TDB3LYP/Lanl2dz approach.

Species (symmetry, spin state)	E_{HOMO}, eV (gas phase; toluene)	E_{LUMO}, eV (gas phase; toluene)	Gap, (eV)	E_{max} (eV)	λ_{max} (nm)
Cd_6Te_6 (C_{3v} ^1A)	–6.15	–3.10	3.05	3.13	395
	–5.97	–2.83	3.14	3.21	386
Cd_8Te_8 (S_4 ^1A)	–6.18	–3.09	3.09	3.22	385
	–6.03	–2.86	3.17	3.25	378
Cd_9Te_9 (D_{3h} ^1A)	–5.94	–3.18	2.76	2.93	423
	–5.76	–2.93	2.83	2.95	420

TABLE 3 | Calculated vertical and adiabatic IPs and EAs (eV) in the gas phase of bare Cd_nTe_n (n = 6, 8, and 9) QDs and capped $Cd_nTe_nL_n$ QDs (where L = TP, MBT, MBN, and MBA) using B3LYP/Lanl2dz level of theory.

Species (symmetry, spin state)	IP_v/IP_{ad}, (eV)	EA_v/EA_{ad}, (eV)
Cd_6Te_6 (C_{3v} ^1A)	7.41/7.21	1.96/2.11
$Cd_6Te_6(TP)_6$ (C_1 ^1A)	6.78/6.30	2.64/3.55
$Cd_6Te_6(MBT)_6$ (C_1 ^1A)	6.34/5.93	2.52/3.44
$Cd_6Te_6(MBN)_6$ (C_1 ^1A)	7.41/6.99	3.34/4.25
$Cd_6Te_6(MBA)_6$ (C_1 ^1A)	7.46/7.24	3.38/4.22
Cd_8Te_8 (S_4 ^1A)	7.33/7.10	2.07/2.17
$Cd_8Te_8(TP)_8$ (C_1 ^1A)	6.61/6.10	2.76/4.16
$Cd_8Te_8(MBT)_8$ (C_1 ^1A)	6.20/5.65	2.71/3.73
$Cd_8Te_8(MBN)_8$ (C_1 ^1A)	7.13/6.71	3.44/4.51
$Cd_8Te8(MBA)_8$ (C_1 ^1A)	7.20/6.75	3.49/4.52
Cd_9Te_9 (D_{3h} $^1A_1$)	7.04/6.96	2.15/2.29
$Cd_9Te_9(TP)_9$ (C_1 ^2A)	6.57/5.72	2.95/4.16
$Cd_9Te_9(MBT)_9$ (C_1 ^2A)	6.28/5.86	2.89/3.68
$Cd_9Te_9(MBN)_9$ (C_1 ^2A)	7.21/6.84	3.53/4.39
$Cd_9Te_9(MBA)_9$ (C_1 ^2A)	7.28/6.98	3.67/2.29

symmetric structures of bare and capped QDs were optimized without symmetry constraints. Vibrational frequency analysis indicated that optimized QD structures are actual minimum energy structures.

All the calculations were performed using hybrid functional B3LYP (Becke, 1993) with basis sets of Los Alamos double-ζ effective core potential (Lanl2dz) (Hay and Wadt, 1985a; Hay and Wadt, 1985b; Wadt et al., 1985) in the gas phase as implemented in the Gaussian 09W package. Earlier studies had found the B3LYP/Lanl2dz level of theory to be a practical approach in terms of accuracy and efficiency when used to study CdTe and CdSe bare and capped QDs (Kuznetsov et al., 2012; Lim et al., 2012; Kuznetsov and Beratan, 2014). However, utilizing the B3LYP functional may underestimate the HOMO-LUMO gaps and excited-state energy, which may be corrected by using range-separated functionals, as shown in previous studies (Salzner and Aydin, 2011; Kurban et al., 2019; Muz and Kurban, 2020). In small-sized QDs, all the cadmium atoms are exposed to the surface and potentially coordinated with ligands. We also varied the number of ligands attached to QDs to explore the effect of ligand density on the structural and electronic properties of QDs. Theoretical studies were simulated in toluene solvent (dielectric constant ε = 2.2706). The ligand-binding energies (BE) were calculated with the help of the following equation:

$$BE = [E(Cd_nTe_nL_n) - (E(Cd_nTe_n) + nE(L))]/n$$

Where $E(Cd_nTe_nL_n)$ is the energy of capped QD, $E(Cd_nTe_n)$ is the energy of bare QD, and E(L) is the energy of the capping agent. Time-dependent DFT calculations were performed using the B3LYP/Lanl2dz approach both in the gas and implicit solvent to study the electronic transitions of both bare and capped QDs. Calculated spectra were plotted with the help of Gabedit 2.5.0 (Allouche, 2011) to determine λ_{max}/E_{max} from plots. Molecular structures and orbitals were visualized using Molden 5.8 (Schaftenaar and Noordik, 2000) and GaussView, respectively.

RESULTS AND DISCUSSION

Bare Cd_nTe_n (n = 6,8 and 9) Quantum Dots

Figure 2 shows the minimum energy structures of bare Cd_6Te_6, Cd_8Te_8, and Cd_9Te_9 QDs in the gas phase and their Frontier

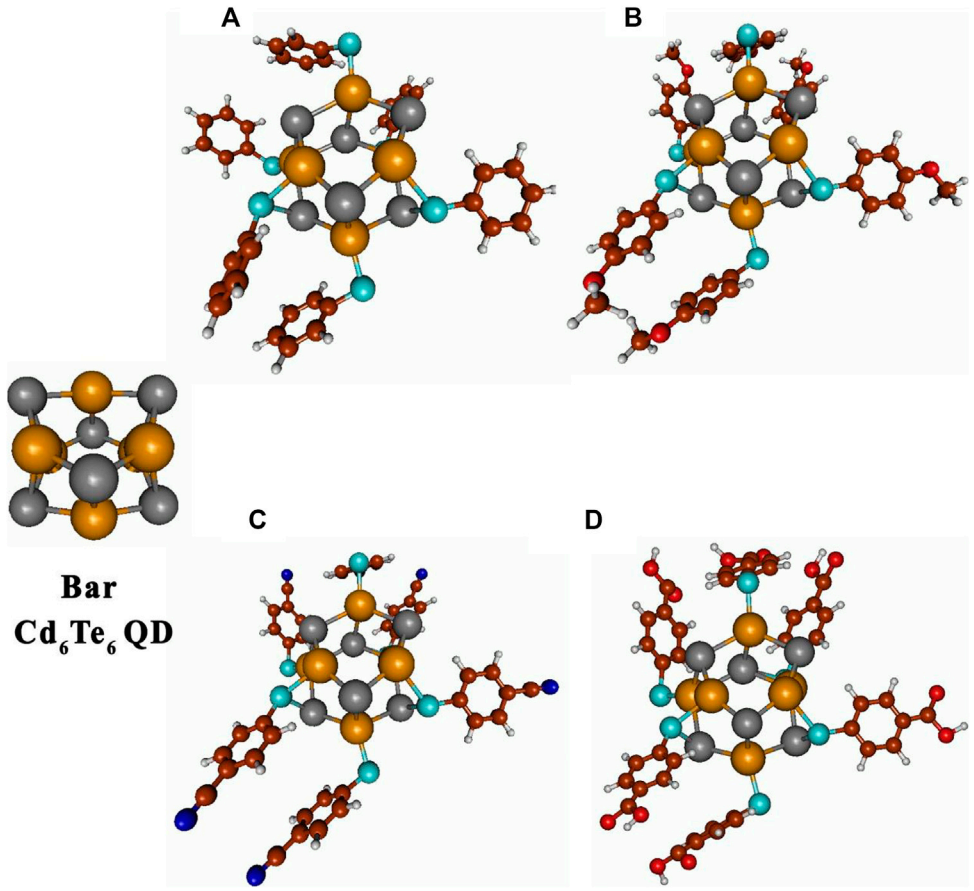

FIGURE 3 | Optimized gas-phase structures of bare and capped Cd_6Te_6 QDs: $Cd_6Te_6(TP)_6$ **(A)**, $Cd_6Te_6(MBT)_6$ **(B)**, $Cd_6Te_6(MBN)_6$ **(C)**, and $Cd_6Te_6(MBA)_6$ **(D)**. Atoms are represented as follows: Cd by dark yellow spheres, Te by dark gray spheres, C brown spheres, H light gray sphere, O red spheres, S sapphire spheres, and N blue spheres.

molecular orbitals. **Table 2** shows calculated HOMO/LUMO energies, HOMO-LUMO gaps, E_{max}, and λ_{max}.

Cd_6Te_6 (C_{3v} symmetry) structure shows that it consists of stacks of Cd_3Te_3 rings of hexagonal shape with a Cd-Te bond distance of 2.87 Å inside the hexagonal rings Cd-Te bond distance between the two layers is 3.045 Å.

Cd-Te bond lengths in Cd_8Te_8 (S_4 symmetry) are calculated to be 2.856–3.002 Å in distorted six Cd_2Te_2 rhombi and four Cd_3Te_3 hexagonal rings.

Cd_9Te_9 (D_{3h} symmetry) consists of three interconnected Cd_3Te_3 hexagonal rings, and Cd-Te bond lengths in upper and lower hexagonal layers are 2.85 Å, while in the middle layer, Cd-Te bond lengths expand to 2.994 Å. The interlayer Cd-Te bond lengths are calculated to be 3.163 Å which is greater than the interlayer bond length of Cd_6Te_6 QD.

Geometry optimization with implicit solvent (toluene) and gas-phase gave similar geometries for all QDs. However, the amount of NBO charges on Cd and Te atoms increased by adding implicit solvent (toluene) during calculations.

In the gas phase, HOMO-LUMO gaps of Cd6Te6, Cd8Te8, and Cd9Te9 QDs revealed that all the QDs were semiconductor-like (**Table 1**). The calculated HOMO-LUMO gaps are 3.05, 3.09, and 2.76 eV for Cd_6Te_6, Cd_8Te_8, and Cd_9Te_9 QDs. Generally, an increase in the size of QDs decreases HOMO-LUMO gaps, but in the present study, HOMO-LUMO gaps of Cd_9Te_9 QD are less than Cd_6Te_6 QD while Cd_8Te_8 QD shows a higher HOMO-LUMO gap than the other two species. We attribute this observation to different structural motifs of each size of QD. Cd_6Te_6 and Cd_9Te_9 are similar to wurtzite structures with six atoms in a ring, whereas Cd_8Te_8 is somewhat similar to zinc-blende structures. Probably this structural difference is the reason behind the unexpected higher bandgap of Cd_8Te_8.

Table 2 presents TD-DFT calculations of excitation energies (E_{max}) and absorption wavelengths (λ_{max}) of excited states with maximum oscillator strength. The calculated excitation energies (E_{max}) of bare QDs in the gas phase are close to the HOMO-LUMO gaps of the same QDs and consistent with the previous computational report

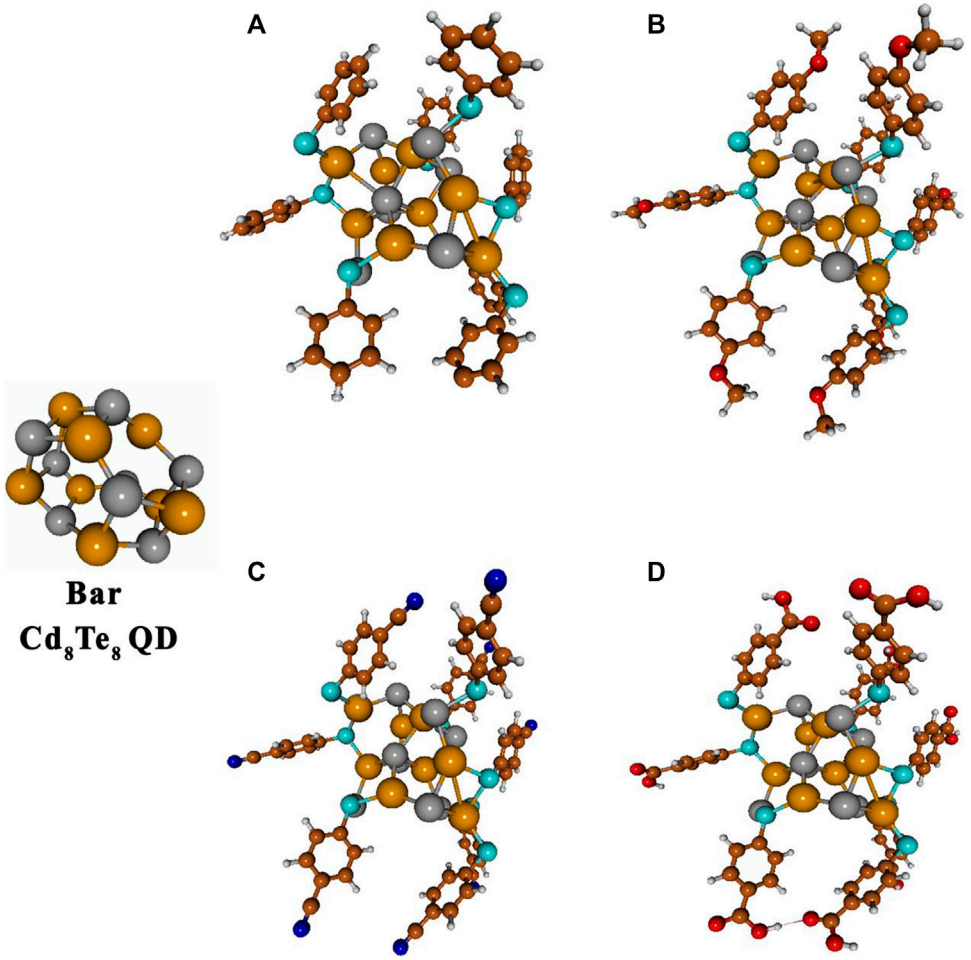

FIGURE 4 | Optimized gas-phase structures of bare and capped Cd_8Te_8 QDs: $Cd_8Te_8(TP)_8$ **(A)**, $Cd_8Te_8(MBT)_8$ **(B)**, $Cd_8Te_8(MBN)_8$ **(C)**, and $Cd_8Te_8(MBA)_8$ **(D)**. Atoms are represented as follows: Cd by dark yellow spheres, Te by dark gray spheres, C brown spheres, H light gray sphere, O red spheres, S sapphire spheres, and N blue spheres.

(Lim et al., 2012). The inclusion of toluene solvent in calculations slightly increased the excitation energies. A blue shift in the absorption maxima caused by the solvent is an interesting observation. One may find few previously published studies on solvents' effect on the absorption spectrum of CdSe clusters reporting a blue shift occurrence (Xu et al., 2010a; Xu et al., 2010b; Lim et al., 2012). In our research, we have observed a similar blue shift occurrence in the case of CdTe clusters.

IP_v and EA_v values are considered to be an index of stability of QDs. It is energetically not favorable for QDs with large IP_v and EA_v values to be activated toward a chemical reaction. Hence, QDs with large IP_v and EA_v values can be considered more stable. Calculated IP_v/IP_{ad} values and EA_v/EA_{ad} values are given in **Table 3**. It is observed that IP_v/IP_{ad} values decrease with an increase in the size of bare QDs, while EAv/EAad values increase gradually with an increase in the size of bare QDs.

Capped Cd_nTe_n (n = 6,8 and 9) Quantum Dots

We capped CdTe QDs with aromatic thiol-radical ligands: TP (C_6H_5S-), MBT ($CH_3OC_6H_4S$-), MBN (CNC_6H_4S-), and MBA ($COOHC_6H_4S$-), (see **Figure 1**). The aromatic ligands were coordinated to the QDs *via* sulfur, which significantly changed the geometries of bare QDs after geometry relaxation. We explored different numbers of capping ligands and different modes of ligands' coordination with QD.

$Cd_6Te_6L_6$ and $Cd_6Te_6L_4$ (L = TP, MBT, MBN, and MBA) species gave stable and physically acceptable geometry after geometry relaxation. For both $Cd_6Te_6L_6$ and $Cd_6Te_6L_4$ species, different geometries arose from bare QD because of Cd-Te bond breakage and Cd-S-Te bridge formation in the form of a 5-membered ring. However, the overall structural motif remained intact, containing interconnected two hexagonal (6-membered rings) layers (see **Figure 3** and **Supplementary Figure S1**).

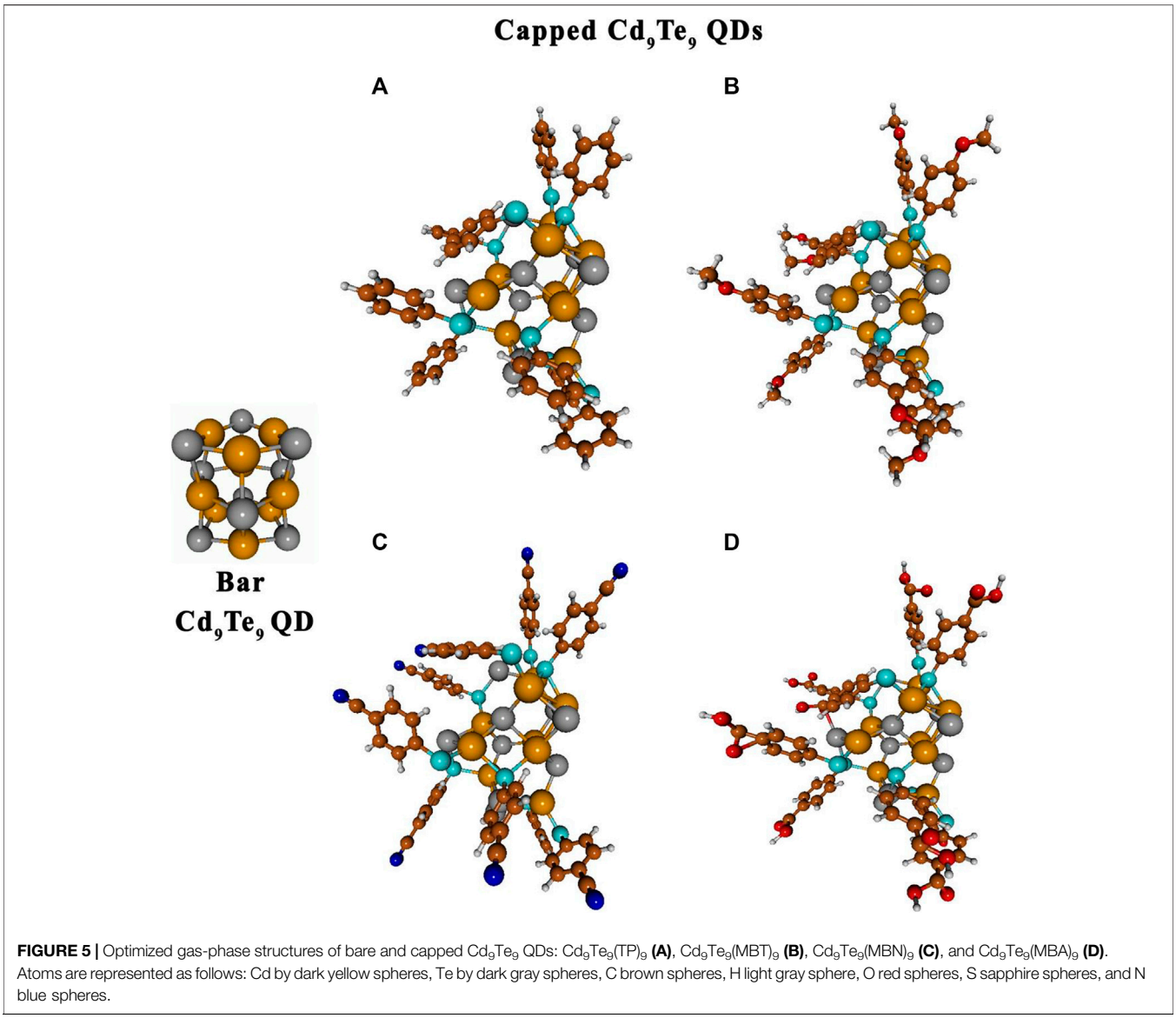

FIGURE 5 | Optimized gas-phase structures of bare and capped Cd_9Te_9 QDs: $Cd_9Te_9(TP)_9$ **(A)**, $Cd_9Te_9(MBT)_9$ **(B)**, $Cd_9Te_9(MBN)_9$ **(C)**, and $Cd_9Te_9(MBA)_9$ **(D)**. Atoms are represented as follows: Cd by dark yellow spheres, Te by dark gray spheres, C brown spheres, H light gray sphere, O red spheres, S sapphire spheres, and N blue spheres.

TABLE 4 | Ligand's total net charge change and net charge change per ligand (in e unit) for capped $Cd_nTe_nL_n$ (n = 6, 8, and 9) QDs (where L = TP, MBT, MBN, and MBA) calculated with B3LYP/Lanl2dz approach in the gas phase.

Ligands		Capped-QDs		
		Cd_6Te_6	Cd_8Te_8	Cd_9Te_9
TP	total	−2.111	−2.596	−3.106
	per ligand	−0.351	−0.324	−0.345
MBT	total	−1.733	−2.388	−2.863
	per ligand	−0.288	−0.298	−0.318
MBN	total	−2.187	−2.716	−3.245
	per ligand	−0.364	−0.339	−0.361
MBA	total	−2.242	−2.932	−3.493
	per ligand	−0.373	−0.366	−0.388

Closed structural configurations were observed after optimization of $Cd_6Te_6L_6$ and $Cd_6Te_6L_4$ species, and these results are different from previous works of Kuznetsov et al. (2012), Lim et al. (2012), where they had capped Cd_6Te_6 with small-sized ligands and observed open structures after geometry relaxation.

The capping of Cd_8Te_8 QDs (with S_4 point group) by all four aromatic ligands led to a slight opening of the bare QD structure due to Cd-Te bond breakage, Cd-S-Cd bridge formation with 4-membered rings, Cd-S-Te bridge formation with 5-membered rings, and formation of one 8-membered ring. We explored the geometries of two $Cd_8Te_8L_8$ and $Cd_8Te_8L_4$ species and found that ligands caused a slight opening of the bare QD structure in both cases. On a relative scale, the coordination of eight ligands caused a larger opening than four ligands (see **Figure 4** and **Supplementary Figure S2**).

Similarly, Cd_9Te_9 QD (with D_{3h} point group) was also capped with the aromatic thiol-radical ligands, which led to significant changes in QD's structure compared to its bare lowest energy structure (see **Figure 5** and **Supplementary Figure S3**). Optimized structures of $Cd_9Te_9L_9$ species showed open

TABLE 5 | E_{HOMO} and E_{LUMO} energies (eV), HOMO-LUMO gaps (eV), and binding energy (BE/L) in kcal/mol of capped $Cd_nTe_nL_n$ (*n* = 6, 8, and 9) QDs (where L = TP, MBT, MBN, and MBA) calculated with B3LYP/Lanl2dz approach.

Species (symmetry, spin state)	E_{HOMO}, (eV)	E_{LUMO}, (eV)	Gap, (eV)	BE/L, kcal/mol
$Cd_6Te_6(TP)_6$ (C_1 ^1A)	–5.57	–3.97	1.6	–17.9
$Cd_6Te_6(MBT)_6$ (C_1 ^1A)	–5.28	–3.72	1.56	–16.6
$Cd_6Te_6(MBN)_6$ (C_1 ^1A)	–6.60	–4.71	1.89	–26.1
$Cd_6Te_6(MBA)_6$ (C_1 ^1A)	–6.22	–4.45	1.77	–36.4
$Cd_8Te_8(TP)_8$ (C_1 ^1A)	–5.62	–3.60	2.02	–19.3
$Cd_8Te_8(MBT)_8$ (C_1 ^1A)	–5.33	–3.41	1.92	–17.5
$Cd_8Te_8(MBN)_8$ (C_1 ^1A)	–6.62	–4.45	2.17	–28.1
$Cd_8Te_8(MBA)_8$ (C_1 ^1A)	–6.60	–4.44	2.16	–30.6
$Cd_9Te_9(TP)_9$ (C_1 ^2A)	*α*:–5.36	*α*: –3.46	*α*: 1.90	–20.9
	β:–5.36	*β*: –4.64	*β*: 0.72	
$Cd_9Te_9(MBT)_9$ (C_1 ^2A)	*α*: –5.11	*α*: –3.09	*α*: 2.02	–19.3
	β: –5.10	*β*: –4.32	*β*: 0.78	
$Cd_9Te_9(MBN)_9$ (C_1 ^2A)	*α*: –6.53	*α*: –4.52	*α*: 2.01	–29.2
	β: –6.53	*β*: –5.57	*β*: 0.96	
$Cd_9Te_9(MBA)_9$ (C_1 ^2A)	*α*: –6.17	*α*: –4.04	*α*: 2.13	–38.8
	β: –6.16	*β*: –5.10	*β*: 1.06	

structures with a hexagonal ring at the center while above and lowered layer opened up to stabilize the structure. It resulted in Cd-Te bond breakage, Cd-S-Cd bridge formation with 4-membered rings, and Cd-S-Te bridge formation with 5-membered rings. However, in the case of $Cd_9Te_9L_4$ species with a smaller number of capping ligands attached to QDs, the closed-shell configuration of Cd_9Te_9 QDs remained intact with the slight opening of the QDs structures. These changes in the structure of capped Cd_9Te_9 QDs also arise from the formation of multiple Cd-S-Te bridges in 5-membered ring configuration and breakage of Cd-Te bonds. These findings are consistent with the previous works of Kuznetsov et al. (2012), Lim et al. (2012).

We performed NBO charge analysis to explore the distribution of charges on QDs after capping with aromatic ligands. Cd atoms in all $Cd_6Te_6L_6$ species displayed positive charges that range from 0.71e to 0.85e. While positive charges on Cd atoms in bare Cd_6Te_6 QDs were 0.76e. There was an increase in the positive charge on Cd atoms in all capped QDs. The ranges of negative charges on Te atoms in capped $Cd_6Te_6L_6$ species were from −0.11e to −0.77e, close to −0.76e charge on Te atoms in bare Cd_6Te_6 QD.

In $Cd_8Te_8L_8$ species, the positive charges on the Cd atoms were also higher than bare Cd_8Te_8 QD. The positive charges on Cd atoms in ligated $Cd_8Te_8L_8$ species were in the range of 0.64e to 0.94e. Compared to bare Cd_8Te_8 QD, there was no significant negative charge change on Te atoms in ligated $Cd_8Te_8L_8$ species. However, those Te atoms which formed a bridge configuration of Cd-S-Te in capped $Cd_8Te_8L_8$ species displayed low negative charges.

In bare Cd_9Te_9 QD, the range of positive charges on Cd atoms and negative charges on Te atoms were (0.71–0.79)e and -(0.72–0.85)e, respectively. The range of positive charges on Cd atoms in $Cd_9Te_9L_9$ species was 0.74e to 0.91e. The negative charges on the Te atom in ligated $Cd_9Te_9L_9$ species varied from −0.05e to −0.87e. Both positive and negative charge distribution in capped $Cd_9Te_9L_9$ species varied tremendously. A significant negative charge accumulates on the oxygen of the methoxy group of MBT, the nitrogen of the nitrile group of MBN, and oxygens of the carboxyl group of MBA.

At the CdTe-ligand interface, the charge interchange between the ligand and the QD produces a dipole layer that could influence the oxidation potential of QDs. The extent of charge transfer between the ligand and the QDs determines the strength of the dipole layer. Adsorption of ligands to the QDs causes a change in the net charge of the capping ligands. **Table 4** presents the total net change in the NBO charge of capping ligands and the net change in the NBO charge per ligand for all capped QDs. A negative value of net charge transfer by ligands indicates that ligands withdraw electron density from the QDs. The net NBO charge change is in the following order: $Cd_nTe_n(MBA)_n$ > $Cd_nTe_n(MBN)_n$ > $Cd_nTe_n(TP)_n$ > $Cd_nTe_n(MBT)_n$ for each value of n.

Calculated ligand binding energies are given in **Table 5**. The ligand-binding energies of all ligated QDs decrease in the following order: $Cd_nTe_n(MBA)_n$ > $Cd_nTe_n(MBN)_n$ > $Cd_nTe_n(TP)_n$ > $Cd_nTe_n(MBT)_n$ for each value of n. A possible explanation of this sequence of ligand binding energies can be the HOMOs, and LUMOs stabilization, and higher IP_v and EA_v values depicted by MBA and MBN capped QDs (see **Table 1**, **2**, and **5**). On the other hand, $Cd_nTe_n(MBT)_n$ and $Cd_nTe_n(TP)_n$ present lower ligand binding energy due to their HOMOs destabilization and low IP_v and EA_v values. These results are also reflected in NBO charge analysis, where MBA exhibits the biggest charge change by withdrawing electrons density from the QDs. Charge analysis also reveals that oxygens of -COOH groups in $Cd_nTe_n(MBA)_n$ possess greater charges about −(0.598–0.787)e compared to the nitrogen of -CN groups in $Cd_nTe_n(MBN)_n$ that shows charges about −(0.308–0.363)e. This could be another reason for higher ligand binding energies of $Cd_nTe_n(MBA)_n$. Our calculated ligand binding energies values are close to the previous findings of Lim and co-workers (Lim et al., 2012), who calculated binding energies with the B3LYP/Lanl2dz approach in the gas phase for Cd_nSe_n/Cd_nTe_n QDs (n = 3,4,6, and 9) capped with SCH_2COOH–, $SCH_2CH_2CO_2H$–, and $SCH_2CH_2NH_2$

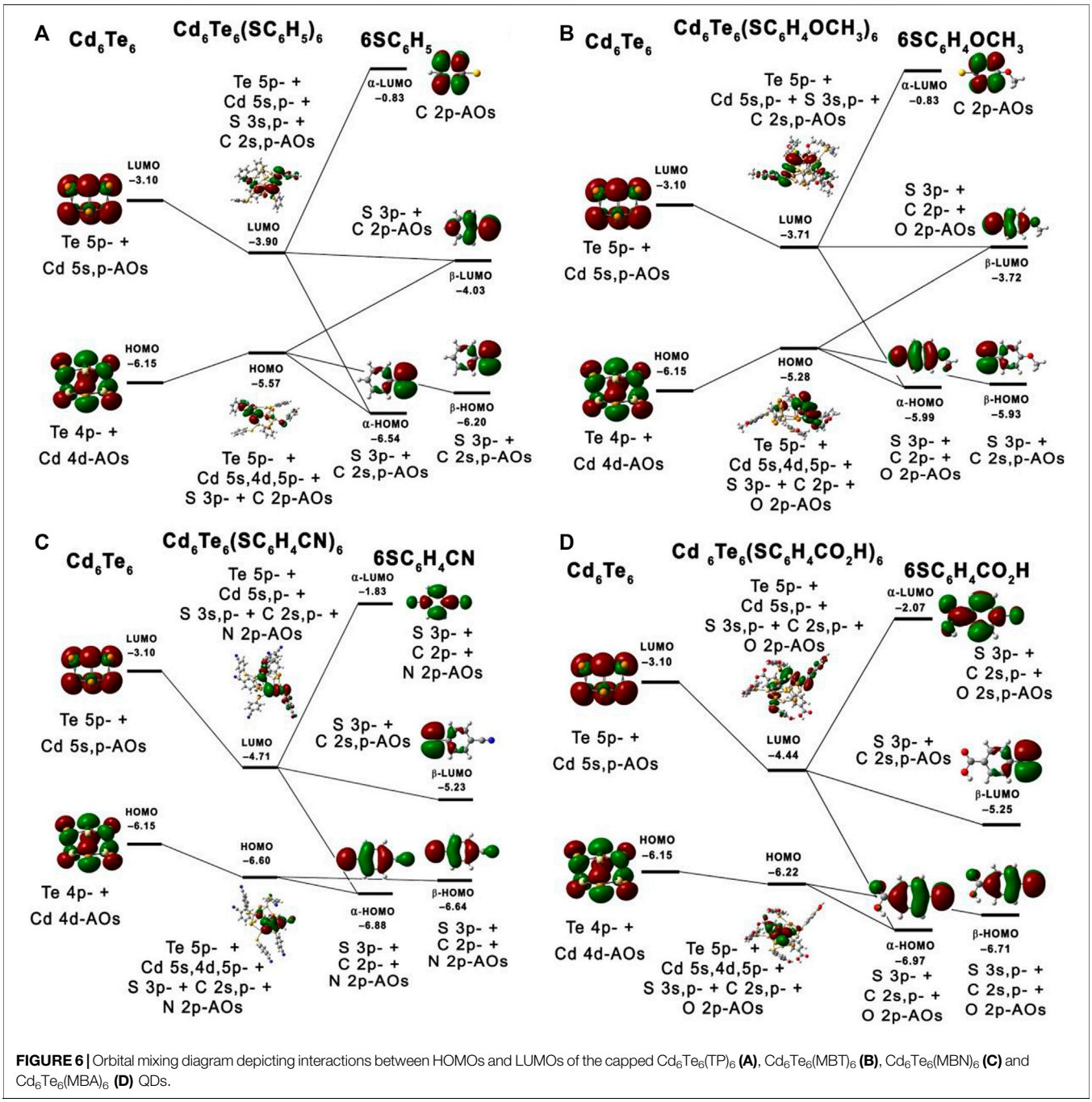

FIGURE 6 | Orbital mixing diagram depicting interactions between HOMOs and LUMOs of the capped $Cd_6Te_6(TP)_6$ **(A)**, $Cd_6Te_6(MBT)_6$ **(B)**, $Cd_6Te_6(MBN)_6$ **(C)** and $Cd_6Te_6(MBA)_6$ **(D)** QDs.

ligands. Our calculated values also agree with the work of Kuznetsov and co-workers (Kuznetsov et al., 2012), who studied Cd_nSe_n/Cd_nTe_n QDs (n = 6,9) capped with NH_3, SCH_3, and OPH_3 ligands in the gas phase using B3LYP/Lanl2dz approach.

Figure 6 presents the interaction of S containing ligands with Cd_6Te_6 QD frontier orbitals. The partial density of states (PDOS) plots (see **Figure 7**) shows the dominant contributions of sulfur 3*p* orbitals of the aromatic thiol-radical ligands in the HOMOs of capped Cd_6Te_6 QDs with minor contributions from QD atoms. On the other hand, the LUMOs of the capped Cd_6Te_6 QD show high contributions from both QD atoms and ligand groups: with slightly higher contributions from Te atoms (see **Figure 7**). The S containing ligands tend to use their lone pair and their unpaired electrons to interact with Cd and Te atoms. An unpaired electron is present in the sulfur 3*p* orbital of thiol-radical ligands. Seemingly, the singly occupied *β*-LUMOs of thiol-radical ligands favorably interact with the doubly occupied HOMO of

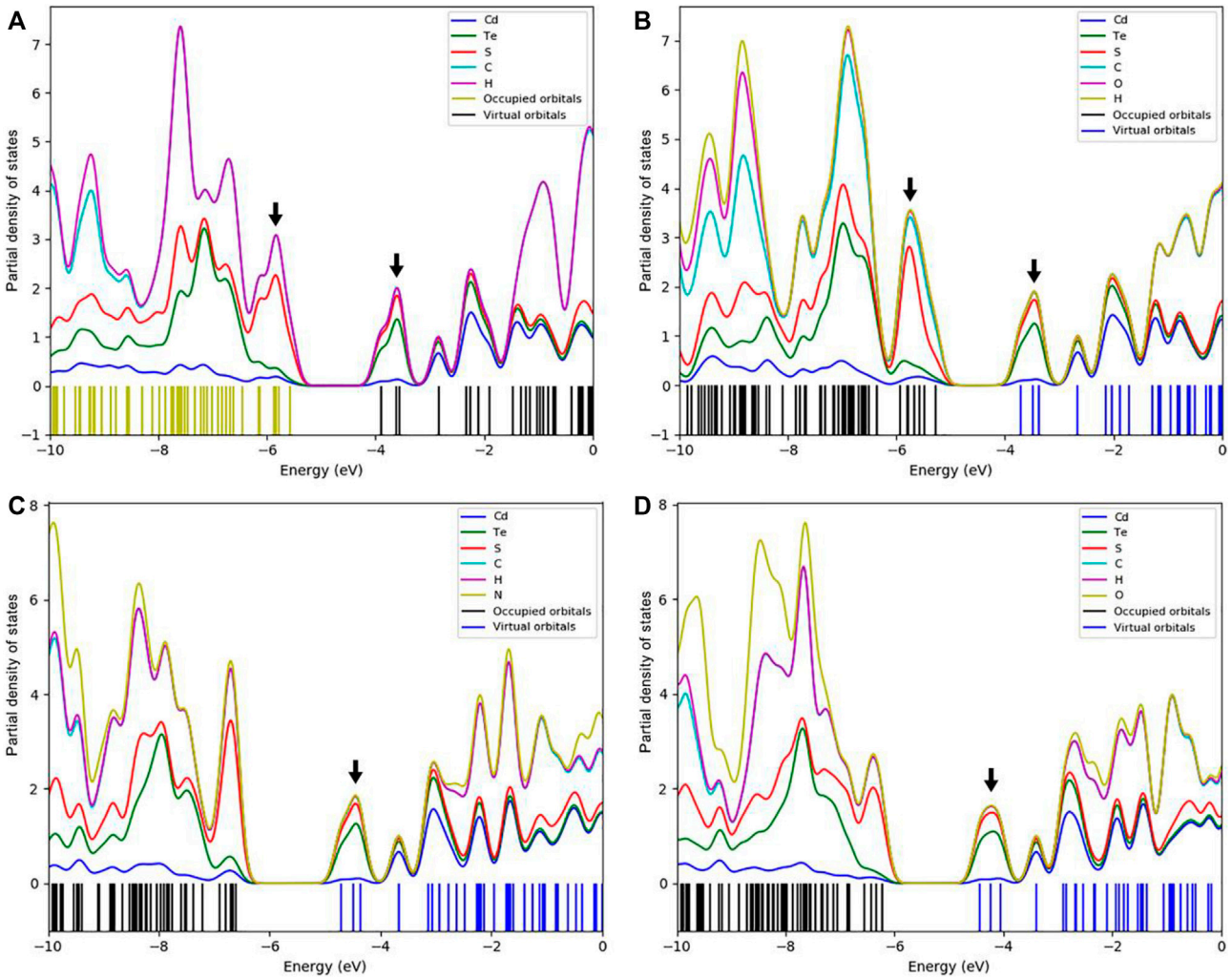

FIGURE 7 | The partial density of states (PDOS) plots (stacked) near the HOMO/LUMO gaps for the capped $Cd_6Te_6(TP)_6$ **(A)**, $Cd_6Te_6(MBT)_6$ **(B)**, $Cd_6Te_6(MBN)_6$ **(C)** and $Cd_6Te_6(MBA)_6$ **(D)** QDs calculated with B3LYP/Lanl2DZ approach.

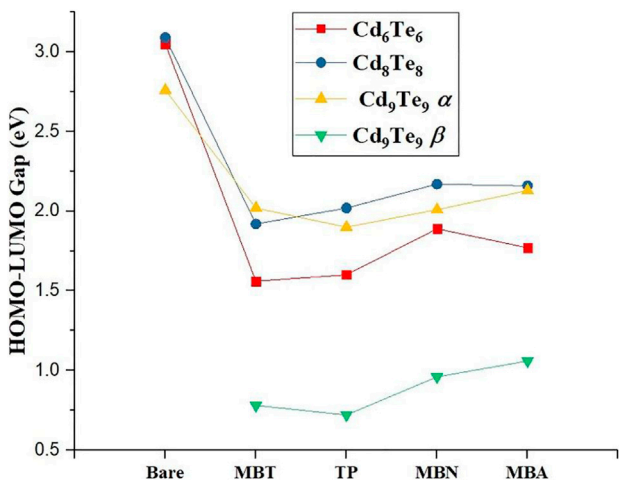

FIGURE 8 | HOMO-LUMO gap (eV) for bare and capped $Cd_nTe_nL_n$ (n = 6, 8, and 9) QDs.

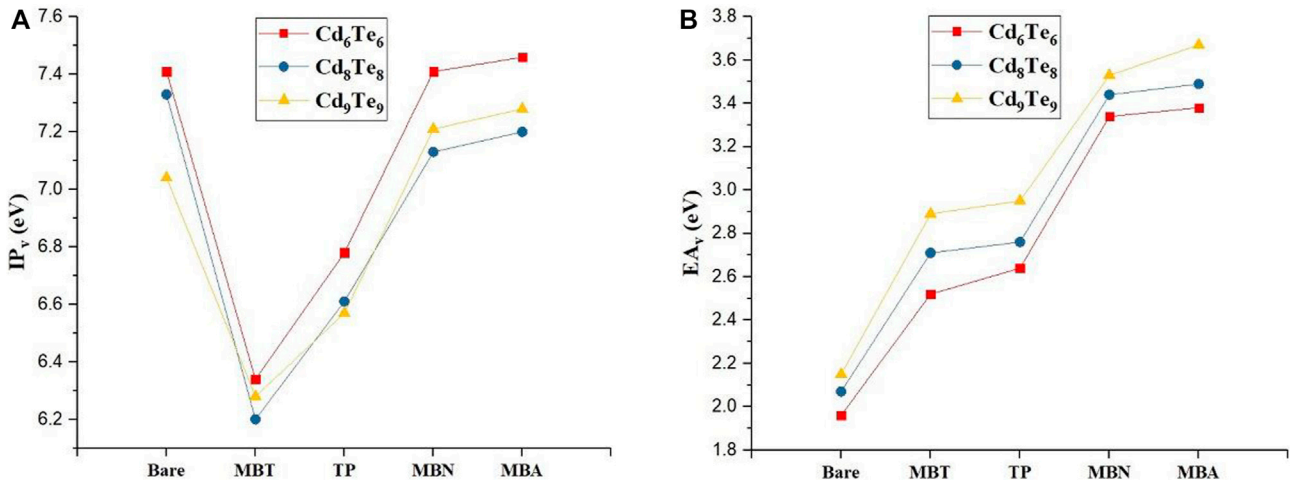

FIGURE 9 | IP_v **(A)** and EA_v **(B)** for bare and capped $Cd_nTe_nL_n$ (*n*=6, 8, and 9) QDs.

the QD, which possesses some d-character from Cd atoms. This interaction destabilizes the HOMO of the capped QDs, as depicted in **Figures 7A,B**. The interaction of the LUMOs of QD with the α-LUMOs and β-LUMOs of thiol-radical ligands highly stabilizes the LUMOs of the capped QDs.

Capping with all four aromatic thiol-radical ligands stabilize the LUMOs of all QDs, while HOMOs are either stabilize or destabilize (see **Tables 2** and **5**). Both TP and MBT ligands destabilize HOMOs in all capped QDs. The effect is much prominent for HOMOs of MBT capped QDs: MBT destabilizes the HOMO by 8.72 eV for Cd_6Te_6, 8.68 eV for Cd_8Te_8, and 8.44 eV for Cd_9Te_9.

On the other hand, both MBN and MBA ligands tend to stabilize HOMOs of all capped QDs. MBN capped QDs show a more pronounced effect with HOMOs stabilization by 4.52 eV for Cd_6Te_6, 4.19 eV for Cd_8Te_8, and 5.82 eV for Cd_9Te_9. All the aromatic thiol-radical ligands decrease the HOMO-LUMO gap of all the capped QDs (see **Tables 2** and **5**) due to the interaction of frontier orbitals of ligands with frontier orbitals of QDs, as shown in **Figure 8**. These observations are due to the stronger stabilization of LUMOs as compared to HOMOs. A drastic decrease in the HOMO-LUMO gap is observed for capped Cd_6Te_6 QDs: 1.45 eV for $Cd_6Te_6(TP)_6$, 1.49 eV for $Cd_6Te_6(MBT)_6$, 1.16 eV for $Cd_6Te_6(MBN)_6$, and 1.28 eV for $Cd_6Te_6(MBA)_6$. While all the other capped QDs show a less pronounced decrease in the HOMO-LUMO gap. This effect of thiol-radical capping ligands is in line with the previous report, where SCH_2COOH, $SCH_2CH_2CO_2H$, and $SCH_2CH_2NH_2$ capped Cd_nSe_n/Cd_nTe_n QDs (n = 3,4,6, and 9) were studied by Lim et al. (2012).

We further explore the effect of aromatic thiol-radical ligands on vertical and adiabatic IPs and EAs of QDs in the gas phase (see **Table 1** and **Figure 9**). Analysis of IP/EA values for bare, and capped QDs reveals that both IP_v/IP_{ad} values show a decrease after capping with all aromatic thiol-radical ligands. However, $Cd_6Te_6(MBA)_6$, $Cd_9Te_9(MBN)_9$, and $Cd_9Te_9(MBA)_9$ species exhibited an increase in IP_v/IP_{ad} values as compared to bare QDs. EA_v/EA_{ad} values increase after capping with all aromatic thiol-radical ligands as compared to bare QDs. It is worth noticing that the capping of QDs with MBT ligand causes the highest decrease in IPv values. Generally, IP_v and EA_v values are considered to be an index of stability of capped-QDs. It is energetically not favorable for QDs with large IP_v and EA_v values to be activated toward a chemical reaction. Hence QDs with large IP_v and EA_v values can be more stable toward a chemical reaction. It is observed that IP_v and EA_v values of capped-QDs decrease in the order MBA > MBN > TP > MBT, so the large IP_v and EA_v values of MBA capped QDs are associated with their higher stability.

The density of states (DOS) plots of thiol-radical ligands revealed the presence of midgap states which were not present in the parent thiol ligands. The conversion of thiol into thiol-radical by dehydrogenation generates one singly occupied *3p* orbital of the sulfur, which appears as midgap states between the HOMO and LUMO states (see **Supplementary Figures S5, S6**). The PDOS plots of $Cd_6Te_6L_6$ species are presented in **Figure 7** as a representative, while DOS plots of the rest of ligands and QDs (both bare and capped species) are given in the supporting information. As indicated in **Figure 7**, the Frontier orbitals of the capped Cd_6Te_6 QDs are mainly composed of ligands' orbitals, which affect the electronic properties of capped QDs, especially the HOMOs and LUMOs energies of the QDs.

To probe the effect of capping on electronic transitions of QDs, we also performed a TD-DFT study. TDB3LYP/Lanl2dz calculations for bare and capped QDs are given in **Tables 3** and **6**. We computed excitation energies (E_{max}), and maximum absorption wavelengths (λ_{max}) for maximum intensity excited states in the gas phase and with implicit solvent (toluene).

All ligated QDs displayed a decrease in excitation energies compared to the excitation energies of their respective bare

TABLE 6 | Calculated E_{HOMO} energy (eV), E_{LUMO} energy (eV), HOMO-LUMO gaps (eV), excitation energies (E_{max}) (eV), and maximum absorption wavelengths (λ_{max}) (nm), of the excited states with maximum oscillator strength of capped $Cd_nTe_nL_n$ (n = 6 and 8) QDs (where L = TP, MBT, MBN, and MBA) in the gas phase and toluene.

Species (symmetry, spin state)	E_{HOMO}, eV (gas phase; toluene)	E_{LUMO}, eV (gas phase; toluene)	Gap, (eV)	E_{max} (eV)	λ_{max} (nm)
$Cd_6Te_6(TP)_6$ (C_1 ^1A)	−5.57	−3.97	1.6	2.59	455
	−5.70	−3.85	1.85	2.88	429
$Cd_6Te_6(MBT)_6$ (C_1 ^1A)	−5.28	−3.72	1.56	2.44	443
	−5.40	−5.71	1.69	2.69	460
$Cd_6Te_6(MBN)_6$ (C_1 ^1A)	−6.60	−4.71	1.89	2.85	434
	−6.52	−4.43	2.09	2.88	443
$Cd_6Te_6(MBA)_6$ (C_1 ^1A)	−6.22	−4.45	1.77	2.81	438
	−6.25	−4.27	1.98	2.83	437
$Cd_8Te_8(TP)_8$ (C_1 ^1A)	−5.62	−3.60	2.02	2.39	465
	−5.74	−3.58	2.16	2.50	495
$Cd_8Te_8(MBT)_8$ (C_1 ^1A)	−5.33	−3.41	1.92	2.31	483
	−5.45	−3.44	2.01	2.30	538
$Cd_8Te_8(MBN)_8$ (C_1 ^1A)	−6.62	−4.45	2.17	2.45	483
	−6.47	−4.20	2.27	2.47	500
$Cd_8Te_8(MBA)_8$ (C_1 ^1A)	−6.60	−4.44	2.16	2.35	482
	−6.40	−4.18	2.22	2.34	529

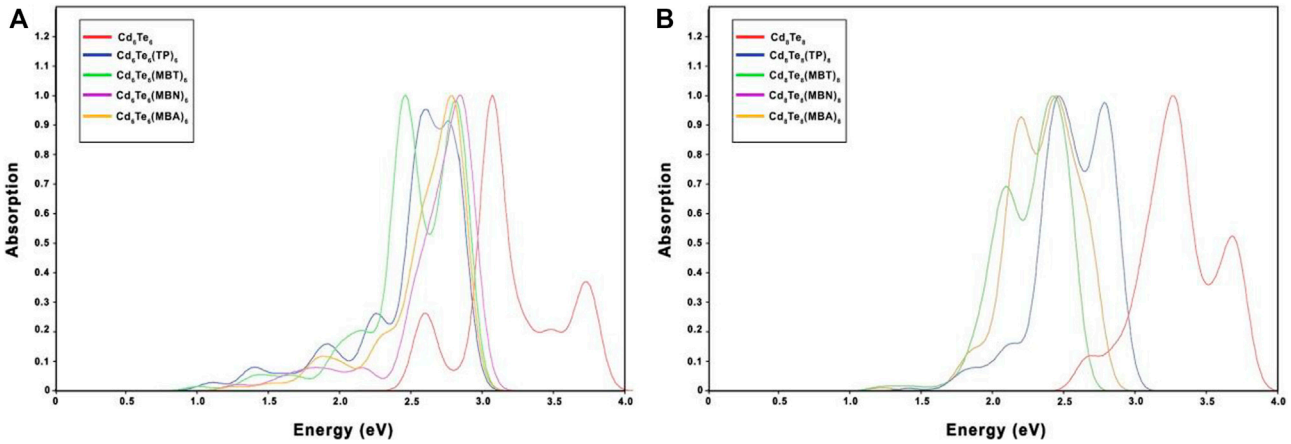

FIGURE 10 | Absorption spectra of bare and capped Cd_6Te_6 **(A)** and Cd_8Te_8 **(B)**, calculated with TDB3LYP/Lanl2DZ approach.

QDs. For capped QDs species, all the thiol-radical ligands altered the absorption spectra of bare Cd_6Te_6 and Cd_8Te_8 QDs by shifting the absorption peaks towards lower energy (redshift) because of the midgap states generated by *3p* orbitals of sulfur, as shown in **Figure 10**. Aromatic ligands are known to influence the electronic and optical properties of QDs by stabilizing the LUMOs and reducing the bandgap. The delocalization of the exciton across the ligand shell is attributed to a significant redshift in the absorption spectra of capped CdTe QDs compared to bare QDs. The ligands' Frontier orbitals coincide with the bandgap of CdTe QDs. Such a resonance situation might generate interfacial QD-ligand states, which would improve the optical properties of the QDs and perhaps open up new relaxation routes for photoexcited charge carriers, hence cause a redshift of the absorption peaks in capped QDs.

The addition of the solvent shifted the redshift toward higher wavelengths for all capped QDs except for $Cd_6Te_6(TP)_6$ and $Cd_6Te_6(MBA)_6$ QDs. It was observed that the redshift in the gas phase for capped-Cd_6Te_6 QDs decreased in the following order: TP > MBT > MBA > MBN. For capped-Cd_8Te_8 QDs, it decreased in the order: MBT ≈ MBN > MBA > TP. These results align with previous studies of similar QDs, which suggested that aromatic thiol ligands cause a redshift of the spectrum (Tan et al., 2012; Nadler and Sanz, 2015; Plata et al., 2017).

CONCLUSION

The effects of aromatic thiol-radical ligands on the structural and electronic properties of Cd_nTe_n quantum dots (n = 6,8,9) were investigated by a systematic DFT study using B3LYP/Lanl2dz

theory level. We chose thiophenol (TP), 4-methoxybenzene-thiol (MBT), 4-mercaptobenzonitrile (MBN), and 4-mercaptobenzoic acid (MBA) as model capping ligands (see **Figure 1**). All the four ligands coordinated to the Cd_nTe_n QDs successfully and formed stable ligand-QD species when subjected to geometry optimization. Generally, the ligands slightly opened up the Cd_6Te_6 and Cd_8Te_8 QDs, but the overall structural motif remained intact. While in the case of Cd_9Te_9, QDs capping with ligands caused the complete opening of the closed structure of bare QDs. Each QDs ligands-QD complexes shows a steady increase in ligand binding energies in the order: MBT < TP < MBN < MBA. The capping of aromatic thiol-radical ligands causes a slight increase in Cd atoms' positive charges due to their electron-withdrawing ability. Adsorption of the ligands decreases the HOMO-LUMO gap due to the stabilization of the LUMOs of QDs. Finally, the TD-DFT study revealed that all the ligands shifted the absorption spectra to redshift in the gas phase and with implicit solvent (toluene).

DATA AVAILABILITY STATEMENT

The original contributions presented in the study are included in the article/**Supplementary Material**, further inquiries can be directed to the corresponding author.

AUTHOR CONTRIBUTIONS

The research idea belongs to MJS. MI performed major computational work. TF and JI have significantly contributed to the discussion and write-up.

SUPPLEMENTARY MATERIAL

The Supplementary Material for this article can be found online at: https://www.frontiersin.org/articles/10.3389/fmats.2021.755332/full#supplementary-material

REFERENCES

Akamatsu, K., Tsuruoka, T., and Nawafune, H. (2005). Band gap Engineering of CdTe Nanocrystals through Chemical Surface Modification. *J. Am. Chem. Soc.* 127 (6), 1634–1635. doi:10.1021/ja044150b

Allouche, A.-R. (2011). Gabedit-A Graphical User Interface for Computational Chemistry Softwares. *J. Comput. Chem.* 32, 174–182. doi:10.1002/jcc.21600

Alnemrat, S., Ho ParkVasiliev, Y. I., and Vasiliev, I. (2014). Ab Initio study of ZnSe and CdTe Semiconductor Quantum Dots. *Physica E: Low-dimensional Syst. Nanostructures* 57, 96–102. doi:10.1016/j.physe.2013.10.037

Amelia, M., Lincheneau, C., Silvi, S., and Credi, A. (2012). Electrochemical Properties of CdSe and CdTe Quantum Dots. *Chem. Soc. Rev.* 41 (17), 5728–5743. doi:10.1039/c2cs35117j

Amin, V. A., Aruda, K. O., Lau, B., Rasmussen, A. M., Edme, K., and Weiss, E. A. (2015). Dependence of the Band Gap of CdSe Quantum Dots on the Surface Coverage and Binding Mode of an Exciton-Delocalizing Ligand, Methylthiophenolate. *J. Phys. Chem. C* 119 (33), 19423–19429. doi:10.1021/acs.jpcc.5b04306

Anikeena, P. O., Halpert, J. E., Bawendi, M. G., and Bulovic, V. (2009). Quantum Dot Light-Emitting Devices with Electroluminescence Tunabe over the Entire Visible Spectrum. *Nano Lett.* 9, 2532–2536. doi:10.1021/nl9002969

Aruda, K. O., Amin, V. A., Thompson, C. M., Lau, B., Nepomnyashchii, A. B., and Weiss, E. A. (2016). Description of the Adsorption and Exciton Delocalizing Properties of P-Substituted Thiophenols on CdSe Quantum Dots. *Langmuir* 32 (14), 3354–3364. doi:10.1021/acs.langmuir.6b00689

Barkhouse, D. A. R., Pattantyus-Abraham, A. G., Levina, L., and Sargent, E. H. (2008). Thiols Passivate Recombination Centers in Colloidal Quantum Dots Leading to Enhanced Photovoltaic Device Efficiency. *ACS Nano* 2 (11), 2356–2362. doi:10.1021/nn800471c

Becke, A. D. (1993). Density-functional Thermochemistry. III. The Role of Exact Exchange. *J. Chem. Phys.* 98 (7), 5648–5652. doi:10.1063/1.464913

Bhattacharya, S. K., and Kshirsagar, A. (2007). Ab Initio calculations of Structural and Electronic Properties of CdTe Clusters. *Phys. Rev. B* 75 (3), 035402. doi:10.1103/physrevb.75.035402

Bhattacharya, S. K., and Kshirsagar, A. (2008). First Principle Study of Free and Surface Terminated CdTe Nanoparticles. *Eur. Phys. J. D* 48 (3), 355–364. doi:10.1140/epjd/e2008-00114-3

Bloom, B. P., Zhao, L.-B., Wang, Y., Waldeck, D. H., Liu, R., Zhang, P., et al. (2013). Ligand-Induced Changes in the Characteristic Size-dependent Electronic Energies of CdSe Nanocrystals. *J. Phys. Chem. C* 117 (43), 22401–22411. doi:10.1021/jp403164w

Bosio, A., Rosa, G., and Romeo, N. (2017). Past, Present and Future of the Thin Film CdTe/CdS Solar Cells. *Sol. Energ.* 175, 31–43. doi:10.1016/j.solener.2018.01.018

Cao, A., Tan, T., Zhang, H., Du, Y., Sun, Y., and Zha, G. (2018). Electronic Structures and Optical Properties of the CdTe/CdS Heterojunction Interface from the First-Principles Calculations. *Physica B: Condensed Matter* 545, 323–329. doi:10.1016/j.physb.2018.06.035

Carey, G. H., Abdelhady, A. L., Ning, Z., Thon, S. M., Bakr, O. M., and Sargent, E. H. (2015). Colloidal Quantum Dot Solar Cells. *Chem. Rev.* 115 (23), 12732–12763. doi:10.1021/acs.chemrev.5b00063

Deng, D., Qu, L., Li, Y., and Gu, Y. (2013). Versatile Self-Assembly of Water-Soluble Thiol-Capped Cdte Quantum Dots: External Destabilization and Internal Stability of Colloidal Qds. *Langmuir* 29, 10907–10914. doi:10.1021/la401999r

Duan, J., Song, L., and Zhan, J. (2009). One-Pot Synthesis of Highly Luminescent CdTe Quantum Dots by Microwave Irradiation Reduction and Their Hg2+-Sensitive Properties. *Nano Res.* 2 (1), 61–68. doi:10.1007/s12274-009-9004-0

Frisch, M. J., Trucks, G. W., Schlegel, H. B., Scuseria, G. E., Robb, M. A., Cheeseman, J. R., et al. (2013). *Gaussian 09, Revision D.01*. Wallingford CT: Gaussian, Inc.

Guo, J., Yang, W., and Wang, C. (2005). Systematic Study of the Photoluminescence Dependence of Thiol-Capped CdTe Nanocrystals on the Reaction Conditions. *J. Phys. Chem. B* 109 (37), 17467–17473. doi:10.1021/jp044770z

Haram, S. K., Kshirsagar, A., Gujarathi, Y. D., Ingole, P. P., Nene, O. A., Markad, G. B., et al. (2011). Quantum Confinement in CdTe Quantum Dots: Investigation through Cyclic Voltammetry Supported by Density Functional Theory (DFT). *J. Phys. Chem. C* 115 (14), 6243–6249. doi:10.1021/jp111463f

Hay, P. J., and Wadt, W. R. (1985). Ab Initio effective Core Potentials for Molecular Calculations. Potentials for the Transition Metal Atoms Sc to Hg. *J. Chem. Phys.* 82 (1), 270–283. doi:10.1063/1.448799

Hay, P. J., and Wadt, W. R. (1985). Ab Initio effective Core Potentials for Molecular Calculations. Potentials for K to Au Including the Outermost Core Orbitals. *J. Chem. Phys.* 82 (1), 299–310. doi:10.1063/1.448975

He, X., and Ma, N. (2014). An Overview of Recent Advances in Quantum Dots for Biomedical Applications. *Colloids Surf. B: Biointerfaces* 124, 118–131. doi:10.1016/j.colsurfb.2014.06.002

Hines, D. A., and Kamat, P. V. (2013). Quantum Dot Surface Chemistry: Ligand Effects and Electron Transfer Reactions. *J. Phys. Chem. C* 117 (27), 14418–14426. doi:10.1021/jp404031s

Hines, D. A., and Kamat, P. V. (2014). Recent Advances in Quantum Dot Surface Chemistry. *ACS Appl. Mater. Inter.* 6 (5), 3041–3057. doi:10.1021/am405196u

Huang, J., Xu, B., Yuan, C., Chen, H., Sun, J., Sun, L., et al. (2014). Improved Performance of Colloidal CdSe Quantum Dot-Sensitized Solar Cells by Hybrid Passivation. *ACS Appl. Mater. Inter.* 6 (21), 18808–18815. doi:10.1021/am504536a

Imran, M., Saif, M. J., Kuznetsov, A. E., Idrees, N., Iqbal, J., and Tahir, A. A. (2019). Computational Investigations into the Structural and Electronic Properties of CdnTen (N = 1-17) Quantum Dots. *RSC Adv.* 9, 5091–5099. doi:10.1039/c8ra09465a

Kanagasubbulakshmi, S., Kathiresan, R., and Kadirvelu, K. (2018). Structure and Physiochemical Properties Based Interaction Patterns of Organophosphorous Pesticides with Quantum Dots: Experimental and Theoretical Studies. *Colloids Surf. A: Physicochemical Eng. Aspects* 549, 155–163. doi:10.1016/j.colsurfa.2018.04.007

Kershaw, S. V., Jing, L., Huang, X., Gao, M., and Rogach, A. L. (2017). Materials Aspects of Semiconductor Nanocrystals for Optoelectronic Applications. *Mater. Horiz.* 4 (2), 155–205. doi:10.1039/c6mh00469e

Kilina, S. V., Tamukong, P. K., and Kilin, D. S. (2016). Surface Chemistry of Semiconducting Quantum Dots: Theoretical Perspectives. *Acc. Chem. Res.* 49 (10), 2127–2135. doi:10.1021/acs.accounts.6b00196

Kumar, S. G., and Rao, K. S. R. K. (2014). Physics and Chemistry of CdTe/CdS Thin Film Heterojunction Photovoltaic Devices: Fundamental and Critical Aspects. *Energy Environ. Sci.* 7 (1), 45–102. doi:10.1039/c3ee41981a

Kumar, A. P., Huy, B. T., Kumar, B. P., Kim, J. H., Dao, V.-D., Choi, H.-S., et al. (2015). Novel Dithiols as Capping Ligands for CdSe Quantum Dots: Optical Properties and Solar Cell Applications. *J. Mater. Chem. C* 3 (9), 1957–1964. doi:10.1039/c4tc01863j

Kurban, M., Gündüz, B., and Göktaş, F. (2019). Experimental and Theoretical Studies of the Structural, Electronic and Optical Properties of BCzVB Organic Material. *Optik* 182, 611–617. doi:10.1016/j.ijleo.2019.01.080

Kuznetsov, A. E., and Beratan, D. N. (2014). Structural and Electronic Properties of Bare and Capped Cd33Se33 and Cd33Te33 Quantum Dots. *J. Phys. Chem. C* 118 (13), 7094–7109. doi:10.1021/jp4007747

Kuznetsov, A. E., Balamurugan, D., Skourtis, S. S., and Beratan, D. N. (2012). Structural and Electronic Properties of Bare and Capped CdnSen/CdnTen Nanoparticles (N = 6, 9). *J. Phys. Chem. C* 116 (12), 6817–6830. doi:10.1021/jp2109187

Leubner, S., Hatami, S., Esendemir, N., Lorenz, T., Joswig, J.-O., Lesnyak, V., et al. (2013). Experimental and Theoretical Investigations of the Ligand Structure of Water-Soluble CdTe Nanocrystals. *Dalton Trans.* 42 (35), 12733–12740. doi:10.1039/c3dt50802a

Liang, H., Song, D., and Gong, J. (2014). Signal-On Electrochemiluminescence of Biofunctional CdTe Quantum Dots for Biosensing of Organophosphate Pesticides. *Biosens. Bioelectron.* 53, 363–369. doi:10.1016/j.bios.2013.10.011

Lim, E., Kuznetsov, A. E., and Beratan, D. N. (2012). Effects of S-Containing Ligands on the Structure and Electronic Properties of CdnSen/CdnTen Nanoparticles (N=3, 4, 6, and 9). *Chem. Phys.* 407, 97–109. doi:10.1016/j.chemphys.2012.09.005

Lin, Y.-C., Chou, W.-C., Susha, A. S., Kershaw, S. V., and Rogach, A. L. (2013). Photoluminescence and Time-Resolved Carrier Dynamics in Thiol-Capped CdTe Nanocrystals under High Pressure. *Nanoscale* 5 (8), 3400–3405. doi:10.1039/c3nr33928a

Lin, X., Xu, S., Wang, C., Wang, Z., and Cui, Y. (2014). Synthesis of Thiosalicylic Acid-Capped CdTe Quantum Dots. *RSC Adv.* 4 (10), 4993–4997. doi:10.1039/c3ra44307h

Liu, F., Laurent, S., Elst, L. V., and Muller, R. N. (2015). Synthesis of CdTe QDs by Hydrothermal Method, with Tunable Emission Fluorescence. *Mater. Res. Express* 2 (9), 95901. doi:10.1088/2053-1591/2/9/095901

Ma, L., Wang, J., and Wang, G. (2012). Search for Global Minimum Geometries of Medium Sized CdnTen Clusters (N=15, 16, 20, 24 and 28). *Chem. Phys. Lett.* 552, 73–77. doi:10.1016/j.cplett.2012.09.036

Muz, İ., and Kurban, M. (2020). The Electronic Structure, Transport and Structural Properties of Nitrogen-Decorated Graphdiyne Nanomaterials. *J. Alloys Compd.* 842, 155983. doi:10.1016/j.jallcom.2020.155983

Nadler, R., and Sanz, J. F. (2015). Effect of Capping Ligands and TiO2 Supporting on the Optical Properties of a (CdSe)13 Cluster. *J. Phys. Chem. A.* 119, 1218–1227. doi:10.1021/acs.jpca.5b00625

Plata, J. J., Ma, A. M., Márquez, A. M., and Sanz, J. F. (2017). Surface on the Electron Injection Mechanism of Copper Sulfide Quantum Dot-Sensitized Solar Cells. *Phys. Chem. Chem. Phys.* 19, 14580–14587. doi:10.1039/C7CP01076A

Rajbanshi, B., Sarkar, S., and Sarkar, P. (2014). Band gap Engineering of Graphene-CdTe Quantum Dot Hybrid Nanostructures. *J. Mater. Chem. C* 2 (42), 8967–8975. doi:10.1039/c4tc01735h

Salzner, U., and Aydin, A. (2011). Improved Prediction of Properties of π-Conjugated Oligomers with Range-Separated Hybrid Density Functionals. *J. Chem. Theor. Comput.* 7 (8), 2568–2583. doi:10.1021/ct2003447

Sarkar, S., Saha, S., Pal, S., and Sarkar, P. (2014). Electronic Structure and Bandgap Engineering of CdTe Nanotubes and Designing the CdTe Nanotube-Fullerene Hybrid Nanostructures for Photovoltaic Applications. *RSC Adv.* 4 (28), 14673–14683. doi:10.1039/c3ra47620k

Schaftenaar, G., and Noordik, J. H. (2000). Molden: A Pre- and Post-Processing Program for Molecular and Electronic Structures. *J. Comput. Aided Mol. Des.* 14, 123–134. doi:10.1023/a:1008193805436

Schnitzenbaumer, K. J., and Dukovic, G. (2018). Comparison of Phonon Damping Behavior in Quantum Dots Capped with Organic and Inorganic Ligands. *Nano Lett.* 18, 3667–3674. doi:10.1021/acs.nanolett.8b00800

Seal, P., Sen, S., and Chakrabarti, S. (2010). Ab Initio investigation on the Nonlinear Optical Properties of CdnTen (N = 1–10) Clusters. *Chem. Phys.* 367 (2-3), 152–159. doi:10.1016/j.chemphys.2009.11.014

Shah, E. V., and Roy, D. R. (2014). A Comparative DFT Study on Electronic, Thermodynamic and Optical Properties of telluride Compounds. *Comput. Mater. Sci.* 88, 156–162. doi:10.1016/j.commatsci.2014.03.013

Sriram, S., and Chandiramouli, R. (2013). DFT Studies on the Stability of Linear, Ring, and 3D Structures in CdTe Nanoclusters. *Res. Chem. Intermed* 41 (4), 2095–2124. doi:10.1007/s11164-013-1334-6

Swenson, N. K., Ratner, M. A., and Weiss, E. A. (2016). Computational Study of the Influence of the Binding Geometries of Organic Ligands on the Photoluminescence Quantum Yield of CdSe Clusters. *J. Phys. Chem. C* 120 (12), 6859–6868. doi:10.1021/acs.jpcc.5b12770

Talapin, D. V., Lee, J.-S., Kovalenko, M. V., and Shevchenko, E. V. (2010). Prospects of Colloidal Nanocrystals for Electronic and Optoelectronic Applications. *Chem. Rev.* 110 (1), 389–458. doi:10.1021/cr900137k

Tan, Y., Jin, S., and Hamers, R. J. (2012). Influence of Hole-Sequestering Ligands on the Photostability of CdSe Quantum Dots. *J. Phys. Chem. C* 117, 313–320. doi:10.1021/jp309587k

Tu, C. C., and Lin, L. Y. (2008). High Efficiency Photodetectors Fabricated by Electrostatic Layer-By-Layer Self-Assembly of CdTe Quantum Dots. *Appl. Phys. Lett.* 93 (16), 6–9. doi:10.1063/1.3003883

Wadt, W. R., Hay, P. J., Wadt, W. A., and Hay, P. J. (1985). Ab Initio effective Core Potentials for Molecular Calculations. Potentials for Main Group Elements Na to Bi. *J. Chem. Phys.* 82, 284–298. doi:10.1063/1.448800

Wang, J., Ma, L., Zhao, J., and Jackson, K. A. (2009). Structural Growth Behavior and Polarizability of CdnTen (N=1-14) Clusters. *J. Chem. Phys.* 130 (21), 214307. doi:10.1063/1.3147519

Weng, J., Song, X., Li, L., Qian, H., Chen, K., Xu, X., et al. (2006). Highly Luminescent CdTe Quantum Dots Prepared in Aqueous Phase as an Alternative Fluorescent Probe for Cell Imaging. *Talanta* 70 (2), 397–402. doi:10.1016/j.talanta.2006.02.064

Wu, Z., Zhang, Y., Huang, S., and Zhang, S. (2013). Theoretical Investigation of Assembled (CdTe)12×N (N=1-5) Multi-Cage Nanochains. *Comput. Mater. Sci.* 68, 238–244. doi:10.1016/j.commatsci.2012.10.040

Wuister, S. F., Swart, I., van Driel, F., Hickey, S. G., and de Mello Donegá, C. (2003). Highly Luminescent Water-Soluble CdTe Quantum Dots. *Nano Lett.* 3 (4), 503–507. doi:10.1021/nl034054t

Wuister, S. F., de Mello Donegá, C., and Meijerink, A. (2004). Local-Field Effects on the Spontaneous Emission Rate of CdTe and CdSe Quantum Dots in Dielectric media. *J. Chem. Phys.* 121, 4310–4315. doi:10.1063/1.1773154

Xiao, J.-W., Ma, S., Yu, S., Zhou, C., Liu, P., Chen, Y., et al. (2018). Ligand Engineering on CdTe Quantum Dots in Perovskite Solar Cells for Suppressed Hysteresis. *Nano Energy* 46, 45–53. doi:10.1016/j.nanoen.2018.01.035

Xu, S., Wang, C., and Cui, Y. (2010). Theoretical Simulation of CdTe Nanocrystals in Aqueous Synthesis. *Struct. Chem.* 21 (3), 519–525. doi:10.1007/s11224-009-9580-3

Xu, S., Wang, C., and Cui, Y. (2010). Theoretical Investigation of CdSe Clusters: Influence of Solvent and Ligand on Nanocrystals. *J. Mol. Model.* 16, 469–473. doi:10.1007/s00894-009-0564-4

Yaacobi-Gross, N., Garphunkin, N., Solomeshch, O., Vaneski, A., Susha, A. S., Rogach, A. L., et al. (2012). Combining Ligand-Induced Quantum-Confined Stark Effect with Type II Heterojunction Bilayer Structure in CdTe and CdSe Nanocrystal-Based Solar Cells. *ACS Nano* 6 (4), 3128–3133. doi:10.1021/nn204910g

Yaghini, E., Seifalian, A. M., and MacRobert, A. J. (2009). Quantum Dots and Their Potential Biomedical Applications in Photosensitization for Photodynamic Therapy. *Nanomedicine* 4 (3), 353–363. doi:10.2217/nnm.09.9

Zheng, Y., Gao, S., and Ying, J. Y. (2007). Synthesis and Cell-Imaging Applications of Glutathione-Capped CdTe Quantum Dots. *Adv. Mater.* 19 (3), 376–380. doi:10.1002/adma.200600342

Zou, H., Liu, M., Zhou, D., Zhang, X., Liu, Y., Yang, B., et al. (2017). Employing CdSexTe1-X Alloyed Quantum Dots to Avoid the Temperature-Dependent

Emission Shift of Light-Emitting Diodes. *J. Phys. Chem. C* 121 (9), 5313–5323. doi:10.1021/acs.jpcc.6b12129

Conflict of Interest: The authors declare that the research was conducted in the absence of any commercial or financial relationships that could be construed as a potential conflict of interest.

Publisher's Note: All claims expressed in this article are solely those of the authors and do not necessarily represent those of their affiliated organizations, or those of the publisher, the editors and the reviewers. Any product that may be evaluated in this article, or claim that may be made by its manufacturer, is not guaranteed or endorsed by the publisher.